Contact efflorescence as a pathway for crystallization of atmospherically relevant particles

Ryan D. Davis[a,b,1], Sara Lance[a,2], Joshua A. Gordon[c], Shuichi B. Ushijima[a,b], and Margaret A. Tolbert[a,b,1]

[a]Cooperative Institute for Research in Environmental Sciences, University of Colorado Boulder, Boulder, CO 80309; [b]Department of Chemistry and Biochemistry, University of Colorado Boulder, Boulder, CO 80309; and [c]Communications Technology Laboratory, National Institute of Standards and Technology, Boulder, CO 80305

Contributed by Margaret A. Tolbert, November 19, 2015 (sent for review October 2, 2015; reviewed by Allan K. Bertram and Will Cantrell)

Inadequate knowledge of the phase state of atmospheric particles represents a source of uncertainty in global climate and air quality models. Hygroscopic aqueous inorganic particles are often assumed to remain liquid throughout their atmospheric lifetime or only (re)crystallize at low relative humidity (RH) due to the kinetic limitations of efflorescence (salt crystal nucleation and growth from an aqueous solution). Here we present experimental observations of a previously unexplored heterogeneous nucleation pathway that we have termed "contact efflorescence," which describes efflorescence initiated by an externally located solid particle coming into contact with the surface of a metastable aqueous microdroplet. This study demonstrates that upon a single collision, contact efflorescence is a pathway for crystallization of atmospherically relevant aqueous particles at high ambient RH (≤80%). Soluble inorganic crystalline particles were used as contact nuclei to induce efflorescence of aqueous ammonium sulfate [$(NH_4)_2SO_4$], sodium chloride (NaCl), and ammonium nitrate (NH_4NO_3), with efflorescence being observed in several cases close to their deliquescence RH values (80%, 75%, and 62%, respectively). To our knowledge, these observations represent the highest reported efflorescence RH values for microdroplets of these salts. These results are particularly important for considering the phase state of NH_4NO_3, where the contact efflorescence RH (∼20–60%) is in stark contrast to the observation that NH_4NO_3 microdroplets do not homogeneously effloresce, even when exposed to extremely arid conditions (<1% RH). Considering the occurrence of particle collisions in the atmosphere (i.e., coagulation), these observations of contact efflorescence challenge many assumptions made about the phase state of inorganic aerosol.

efflorescence | coagulation | aerosol | climate | air quality

Nucleation of the solid phase from a liquid solution (crystallization) is an important process in pharmaceuticals, manufacturing, and atmospheric science (1). In the atmosphere, the phase state and water content of particulate matter influences both heterogeneous chemistry and the aerosol direct and indirect effect on climate (2–6). Despite its importance, there is no comprehensive understanding of the phase state of atmospheric particulate, and the aerosol radiative forcing remains one of the largest uncertainties in climate predictions (6).

A significant fraction of aqueous atmospheric aerosol contains soluble inorganics such as chlorides, sulfates, and nitrates that can undergo efflorescence, i.e., the process of salt crystallization and water evaporation. Efflorescence often occurs at a significantly lower relative humidity (RH) than the reverse process of deliquescence (2, 7–12). A potent example of this hydration hysteresis is demonstrated with ammonium nitrate (NH_4NO_3), a hygroscopic component of atmospheric aerosol (9–11). $NH_4NO_{3(s)}$ crystals will deliquesce to form an aqueous droplet at ∼62% RH (T = 295 K) (13). However, $NH_4NO_{3(aq)}$ droplets do not homogeneously effloresce even at extremely low RH (∼0%) but instead remain in a metastable liquid state (i.e., supersaturated with respect to the aqueous solute) (2, 9, 10). Thus, many atmospheric chemistry and climate models assume that fully deliquesced inorganic particles such as NH_4NO_3 always remain in the aqueous state or only (re)crystallize at a very low ambient RH (<35%) (7, 14, 15).

Although the deliquescence RH (DRH) and efflorescence RH (ERH) for inorganic salts are well-characterized (2), heterogeneous efflorescence has been less extensively studied. Heterogeneous efflorescence occurs when a solid particle acts as a surface upon which nuclei can form, lowering the overall activation barrier for nucleation (2, 8–10). Analogous to heterogeneous ice formation, the solid particles can either be immersed inside the droplet (immersion mode of nucleation) or may come into contact with the exterior of the droplet (contact mode of nucleation) (16, 17). Past research has shown that immersion of solid particles such as mineral dust can raise the ERH of some salts relative to homogeneous efflorescence, causing the particles to be solid under a wider range of atmospherically relevant RH conditions (8–10). Similar experiments have not been performed to explore contact-mode efflorescence, and it has yet to be established whether contact would have a different effect on efflorescence than immersion.

Although experimental studies of contact efflorescence have been lacking, a recent modeling study (11) considered phase changes of metastable liquid particles upon coagulation with dry solid particles (i.e., contact efflorescence). That study found an appreciable difference in the particle-phase concentrations of semivolatile inorganic species (e.g., NH_4NO_3) and total aerosol liquid water content when contact-induced phase changes were included in the simulation. Those simulation results point toward the potential real-world importance of contact efflorescence. Indeed, metastable liquid particles and crystalline particles of

Significance

Atmospheric particles contain inorganic material that can effloresce to form a crystalline solid. The phase state of atmospheric particles influences the particle's effect on climate and air quality. Despite the importance of particle phase, there is no comprehensive understanding of particle crystallization, and many climate models assume inorganic particles always remain liquid. Our study demonstrates that contact efflorescence, a previously unexplored pathway for crystallization, can lead to the formation of solid particulate at high relative humidity (RH, ∼80%) upon a single collision. Particles then remain crystalline at all relative humidities below their deliquescence point (<80% RH). Such a high efflorescence RH strongly suggests contact efflorescence may be an important atmospheric process to consider further.

Author contributions: R.D.D., S.L., J.A.G., and M.A.T. designed research; R.D.D. and S.B.U. performed research; R.D.D., S.L., J.A.G., and M.A.T. analyzed data; and R.D.D. and M.A.T. wrote the paper.

Reviewers: A.K.B., University of British Columbia; and W.C., Michigan Technological University.

The authors declare no conflict of interest.

[1]To whom correspondence may be addressed. Email: tolbert@colorado.edu or Ryan.Davis-1@colorado.edu.

[2]Present address: Department of Earth, Atmospheric and Planetary Sciences, Massachusetts Institute of Technology, Cambridge, MA 02139.

This article contains supporting information online at www.pnas.org/lookup/suppl/doi:10.1073/pnas.1522860113/-/DCSupplemental.

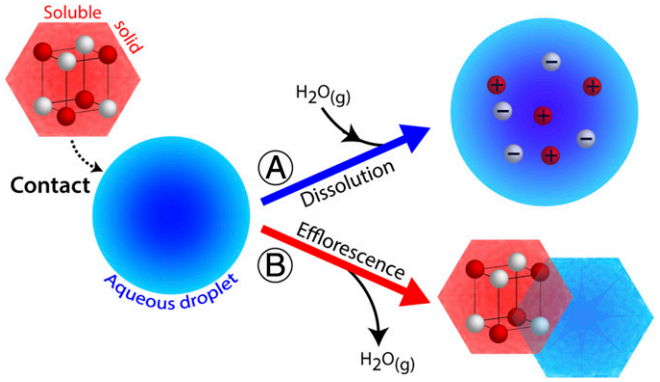

Fig. 1. The potential outcomes of an externally located solid soluble inorganic aerosol coming into contact with a metastable aqueous inorganic microdroplet. In process A, dissolution of the solid particle accompanied by uptake of water. In process B, efflorescence accompanied by evaporation of water.

greatly different compositions can coexist simultaneously in the same air parcel (3, 7, 11, 18, 19). Although immersion efflorescence requires the heterogeneous nuclei to be insoluble or sparingly soluble, there is no such inherent limitation for contact efflorescence. Thus, even highly soluble solid particles can potentially serve as contact nuclei (CN). Alternatively, soluble particles may dissolve upon contact. The contrasting effects of dissolution upon contact compared with efflorescence are illustrated in Fig. 1. Although efflorescence is accompanied by crystallization and water loss, dissolution would be accompanied by droplet growth and water uptake to establish an equilibrium water activity. Reconciling which process preferentially occurs upon contact is thus necessary to predict the phase state and water content of atmospheric particles.

Here, we report on well-controlled experimental observations of contact efflorescence and a discussion of potential implications. To our knowledge, these experiments represent the first observations of contact efflorescence beyond our previous study (12) of aqueous ammonium sulfate [$(NH_4)_2SO_4$] microdroplets seeded with $(NH_4)_2SO_4$ microcrystals. In the present study, highly soluble inorganic salts of atmospheric relevance were used as CN. Due to their high solubility, these CN salts are not typically considered as effective heterogeneous nuclei. We probe the heterogeneous ability of these soluble CN by observing contact efflorescence of aqueous sodium chloride (NaCl), $(NH_4)_2SO_4$, and NH_4NO_3, three atmospherically abundant and important compounds (2–15). The highest single-collision contact efflorescence relative humidity (CERH) was measured for single optically levitated droplets exposed to single collisions with CN. We demonstrate that contact efflorescence is a pathway for crystallization of aqueous inorganic particles at the highest RH at which efflorescence is thermodynamically possible (near their respective DRH).

Materials and Methods

Droplet and CN Composition. Contact efflorescence was studied for optically levitated microdroplets of $(NH_4)_2SO_{4(aq)}$, $NH_4NO_{3(aq)}$, and $NaCl_{(aq)}$ (10 ± 3 μm average droplet diameter) at room temperature (295 ± 1 K). The crystalline compounds used as CN for all three aqueous compositions were potassium sulfate ($K_2SO_{4(CN)}$), sodium sulfate ($Na_2SO_{4(CN)}$), potassium chloride ($KCl_{(CN)}$), sodium bromide ($NaBr_{(CN)}$), $(NH_4)_2SO_{4(CN)}$, and $NaCl_{(CN)}$ (~0.5–1.5 μm dry particle diameter). $NH_4NO_{3(aq)}$ contact efflorescence was further probed using internally mixed CN composed of crystalline NH_4NO_3 and illite dust particles. Contact efflorescence using pure $NH_4NO_{3(CN)}$ was not possible because CN were generated as aqueous droplets and then dried (see *CN Preparation*), but $NH_4NO_{3(aq)}$ microdroplets do not homogeneously effloresce (2, 9, 10). Thus, illite particles were immersed before drying the CN to induce heterogeneous nucleation of the NH_4NO_3 component. NH_4NO_3+illite$_{(CN)}$ was not used for $(NH_4)_2SO_{4(aq)}$ and $NaCl_{(aq)}$ contact efflorescence (see *SI Materials and Methods* for further details).

Droplet Levitation. The entire experimental arrangement is shown in Fig. S1. The optical trap and trapping procedure have been described in detail elsewhere (12). In brief, the optical trap consisted of two vertical counter propagating beams generated using individual continuous-wave Nd:YAG lasers ($\lambda = 532$ nm). The levitation chamber was a black-anodized aluminum flow tube (12-mm inner diameter × 110-mm length) with four window ports at the trapping site (midpoint of the flow tube length). Levitated droplets were generated from a 5 wt% solution of NH_4NO_3, NaCl, or $(NH_4)_2SO_4$ using a piezo-driven device with a 15-μm-diameter orifice (Microfab MJ-APB-015).

CN Preparation. CN were generated as aqueous droplets and then crystallized. Aqueous particles were nebulized into a dry N_2 gas flow using a medical nebulizer (Omron NE-U22) and then directed through a diffusion dryer where the RH was <10% and the particles crystallized. Single-component CN were generated from a 10 wt% aqueous solution of KCl, K_2SO_4, NaCl, NaBr, $(NH_4)_2SO_4$, or Na_2SO_4. NH_4NO_3+illite CN were generated from a solution that was 10 wt% NH_4NO_3 and 5 wt% illite. The nebulizer contained a wire mesh with a pore size of 1 μm × 1 μm that limited the illite particle diameter to ≤ 1 μm.

CN Size. To explore how the size of CN influenced the CERH, $NaCl_{(CN)}$ were size-selected for several trials of $NaCl_{(CN)}$–$(NH_4)_2SO_{4(aq)}$ contact efflorescence using a differential mobility analyzer (DMA). Separate trials were performed for 0.5 μm and 1 μm dry diameter $NaCl_{(CN)}$. For all other CN–droplet combinations, CN were not size-selected, to increase the number concentration of CN and frequency of collisions. Using images of scattered laser light, the polydisperse size distribution of the dry CN was estimated to be ~0.5–1.5 μm dry diameter (see *SI Materials and Methods*). Our previous study (12) of $(NH_4)_2SO_{4(CN)}$–$(NH_4)_2SO_{4(aq)}$ used 1.5-μm seed crystals. Those experiments were repeated here using polydisperse $(NH_4)_2SO_{4(CN)}$.

RH Control and Measurement. The RH within the levitation chamber was controlled by mixing a dry N_2 gas flow with a humidified N_2 gas flow generated using a water bubbler. The flow carrying the dried crystalline particles was mixed with the humidified flow before entering the levitation chamber. The maximum RH achievable while flowing CN was ~77–79%. Two RH probes [Vaisala HMP60, ±0.5 °C, ±3% RH uncalibrated, ±1% RH calibrated (12)] were placed before and after the levitation chamber. The RH at the trapping site was calculated as the average of the two RH measurements (±1 SD, 1–2% RH typical).

Detecting Efflorescence. Efflorescence was detected using far-field imaging of elastically scattered laser light from the 532-nm trapping lasers (12). Light was imaged using a CCD camera. All images were recorded in LabVIEW for postprocessing. As demonstrated in Fig. 2, the far-field images of liquid

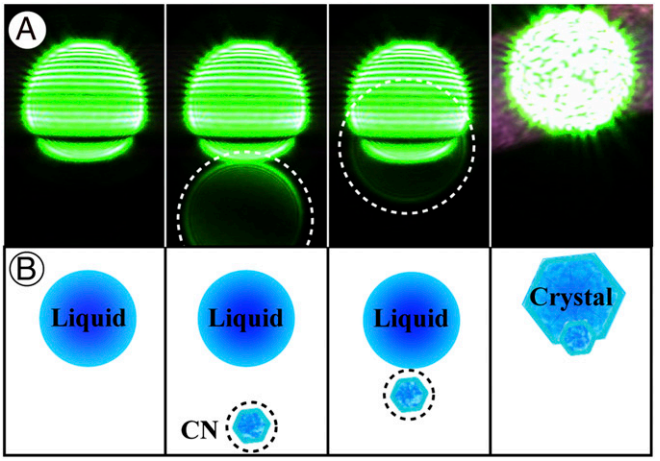

Fig. 2. Observation of $NaCl_{(CN)}$–$(NH_4)_2SO_{4(aq)}$ contact efflorescence at 38% RH (11 ± 2 μm droplet diameter, 0.5 μm CN diameter). (*A*) Far-field imaging of scattered laser light from the trapping lasers. In frame 1, the horizontal linear interference fringes are indicative of a liquid particle. In frame 2, the light scattered off of a CN (encircled by white dashed line) appears at the bottom of the image. In frame 3, the CN has moved closer to the droplet. In frame 4, efflorescence is evident by the breakdown in the linear interference fringes and the upward movement of the particle due to the loss of water mass. (*B*) Illustrated representation of what is shown in each frame of *A*.

droplets contained horizontal linear interference fringes (frames 1–3). Efflorescence is evident by the breakdown in the linear interference fringes and randomization of the laser light phase (frame 4). The number of fringes in an image scaled with droplet size. The diameter of droplets used (~10 ± 3 μm) thus provided a sufficient number of fringes to make the occurrence of efflorescence unambiguous and distinct.

Monitoring Collisions. Collisions were monitored with the 532-nm far-field images (Fig. 2) as well as near-field images of scattered light from a 632.8-nm HeNe probe laser that illuminated the levitated droplet from below. Near-field images provided a clearer picture of CN trajectories, as demonstrated in Fig. S2. A custom LabVIEW image processing program assisted in identifying collisions by searching recorded images for the presence of CN. The velocity at which a CN particle collided with a levitated droplet was kept below ~3 mm/s (total flow rate ≤ 25 sccm), which is an atmospherically realistic value (the mean thermal speed for a 1-μm-diameter particle is ~4 mm/s) (20) and ensured a collision would be captured by the imaging cameras (the camera field-of-view was 200 μm, and ~10 ms elapsed between captured image frames). Six or more images of a CN were typically captured using CN velocities of <3 mm/s.

Determining CERH. The highest single-collision CERH of an aqueous droplet was determined by monitoring collisions and systematically varying the ambient RH whenever efflorescence was not induced by a single collision. Efflorescence was considered to be contact-induced only if it occurred immediately upon contact (i.e., if efflorescence occurred between adjacent recorded images, ~5–10 ms at 100–150 frames per second). If collisions were observed without efflorescence or multiple collisions occurred before efflorescence, a fresh droplet was trapped and a new experiment performed at a slightly lower RH (~0.5–5% RH lower). Once single-collision contact efflorescence was observed, the RH was raised again by ~2–5% RH, and the process was repeated. The average highest single-collision CERH was calculated from two to five trials (±1 SD with propagated error from the individual RH measurements).

Results

The individual results for all CN–droplet contact efflorescence experiments are shown in Dataset S1. The $NaCl_{(CN)}$–$(NH_4)_2SO_{4(aq)}$ contact efflorescence experiments using size-selected $NaCl_{(CN)}$ (0.5 μm and 1 μm dry diameter) were compared with the results using polydisperse $NaCl_{(CN)}$ (~0.5–1.5 μm dry diameter). In each case, the highest single-collision CERH was ~38% regardless of CN size, indicating that any potential CN size dependence is not resolvable over the range of sizes probed. Polydisperse CN were used for the experiments involving all of the other CN–droplet pairs.

The average highest single-collision CERH for all CN–droplet pairs is given in Fig. 3 and plotted on the characteristic hydration hysteresis diagram for each of the aqueous salts. (Hereafter, the use of CERH will refer to the average highest single-collision CERH.) It can be seen that some CN compositions dramatically increase the ERH, whereas others only modestly increase it. A phase transition is only thermodynamically possible below the droplet DRH. Thus, to place the CERH into the context of the range of possible and relevant RH values, a parameter σ(*RH*) is defined as

$$\sigma(RH) = (DRH - CERH)/(DRH - RH_{\min}) \qquad [1]$$

where *DRH* is 75%, 80%, and 62% RH for $NaCl_{(aq)}$, $(NH_4)_2SO_{4(aq)}$, and $NH_4NO_{3(aq)}$, respectively, and RH_{min} is the lowest RH at which a droplet will retain water if no collisions occur. For $(NH_4)_2SO_{4(aq)}$ and $NaCl_{(aq)}$, RH_{min} is the homogeneous ERH (36 ± 2% and 44 ± 2% RH, respectively). $NH_4NO_{3(aq)}$ did not homogeneously effloresce when exposed to extremely arid conditions (<1% RH) for 24 h, consistent with previous studies (9, 10), and always remained liquid if no collisions occurred. Thus, an RH_{min} of 0% was used for $NH_4NO_{3(aq)}$. Average values for σ(*RH*) are included in Fig. 3, with values ranging from near zero to near unity. For instances in which σ(*RH*) ≈ 0, contact efflorescence occurred near the DRH of the droplet (i.e., CERH ≈ DRH, the maximum possible value), indicative of a highly effective CN. When σ(*RH*) ≈ 1, contact did not significantly influence efflorescence relative to the homogeneous case, indicative of a less effective CN. Note that for all instances, the CERH was greater than RH_{min} [σ(*RH*) < 1].

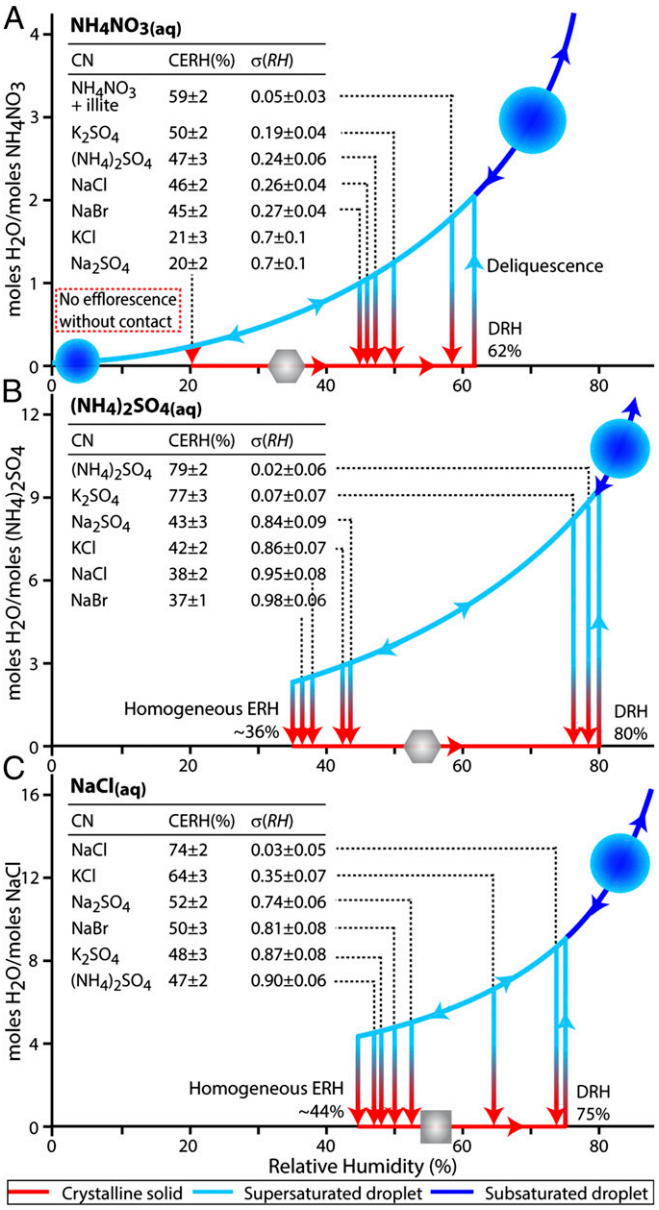

Fig. 3. Contact efflorescence results depicted on characteristic hysteresis diagrams for (*A*) $NH_4NO_{3(aq)}$, (*B*) $(NH_4)_2SO_{4(aq)}$, and (*C*) $NaCl_{(aq)}$. The CERH is indicated for each CN used. In all cases, contact raised the ERH relative to the homogeneous case. Note that, without contact, $NH_4NO_{3(aq)}$ droplets do not homogeneously crystallize at low RH and remain on the hydrated (upper, blue) portion of the curve at all RH values. Aqueous droplets respond to changes in RH by increasing or decreasing in water content. If efflorescence occurs, crystalline particles remain on the dehydrated (lower, red) portion of the curve until the RH is raised to the DRH. Before deliquescence, crystalline particles do not substantially respond to changes in RH. Hydration values (*y* axes, moles H_2O per moles solute) were calculated using the Extended Aerosol Inorganic Model (E-AIM, www.aim.env.uea.ac.uk/aim/aim.php) (13).

Discussion

This study has experimentally demonstrated that a single solid–liquid collision can result in efflorescence of aqueous droplets at RH values significantly above RH_{min} of the pure aqueous component. Importantly, this study has also shown that even highly soluble crystalline particles can induce efflorescence of an

aqueous droplet upon contact. Insolubility is frequently invoked as a requirement for an efficient heterogeneous nucleus (16), but all CN studied here were soluble and also capable of inducing efflorescence. For a given CN–droplet pair, the CERH did not vary more than ±1–2% RH in different trials. However, there was a wide variation in CERH when comparing CN of different compositions, likely due to differences in, e.g., CN crystal lattice structure, hygroscopic properties, solubility, and ionic interactions, as discussed in *Isochemical Contact Efflorescence* and *Heterochemical Contact Efflorescence*.

Isochemical Contact Efflorescence. Crystal nucleation is the initial formation of the new crystalline phase. In the unique cases of isochemical contact efflorescence [i.e., $NaCl_{(CN)}$–$NaCl_{(aq)}$, $(NH_4)_2SO_{4(CN)}$–$(NH_4)_2SO_{4(aq)}$, and NH_4NO_3+illite$_{(CN)}$–$NH_4NO_{3(aq)}$], nucleation is not necessary because the seed crystal is of the same composition as the anticipated crystalline phase. In theory, crystal growth and subsequent loss of water (i.e., efflorescence) is therefore expected at all levels of supersaturation (any RH < DRH) if the seed crystal is larger than a critical cluster ($\lesssim$ 10 nm) (21). As expected, the CERH was close to the DRH in all three isochemical cases. In each case, the CERH was slightly below the DRH due to experimental limitations and the uncertainty associated with the RH probes (±1%). It is likely that the true CERH values are closer to the DRH than reported here.

Heterochemical Contact Efflorescence. Similarity in crystal lattice structure between the heterogeneous surface and the crystallizing compound has long been recognized as an important factor in heterogeneous nucleation (16, 22–24). Here, we explore the strength of this relationship by comparing crystal lattice structure and σ(*RH*). $NH_4NO_{3(s)}$, $(NH_4)_2SO_{4(s)}$, $Na_2SO_{4(s)}$, and $K_2SO_{4(s)}$ have orthorhombic lattice structures, whereas $NaCl_{(s)}$, $NaBr_{(s)}$, and $KCl_{(s)}$ are cubic. A scaled representation of the unit cell structures for each salt is shown in Fig. 4*A*, with values for the unit cell constants *a*, *b*, and *c* given in Table S1. The standard expression for lattice mismatch (δ) between a substrate (i.e., the CN) and a crystalizing overlayer (i.e., the aqueous component) is given by $\delta = (a_{CN} - a_{aq})/a_{aq}$, where a_{aq} is the lattice constant of the crystalline phase of the droplet component and a_{CN} is the lattice constant of the CN (22–24). This equation was valid for cases where both species were cubic crystals. For the orthorhombic crystals, the lattice constants are not equal, and it is necessary to account for lattice mismatch in mutually perpendicular directions (22). Thus, δ was calculated as the average absolute mismatch of the lattice constants a_1 and a_2 of the (001), (010), and (100) crystal faces, as given by

$$\delta = \left[\left|\left(a_{1,CN} - a_{1,aq}\right)/a_{1,aq}\right| + \left|\left(a_{2,CN} - a_{2,aq}\right)/a_{2,aq}\right|\right]/2. \quad [2]$$

The orientation of these crystal faces is depicted in Fig. 4*A*. The crystal faces that yielded the lowest value of δ were used. (See *SI Materials and Methods* and Fig. S3 for further details and discussion of calculating δ with integer multiplication of a_1 and a_2.) Subscripts for δ of AS, AN, or SC specify the aqueous phase as $(NH_4)_2SO_{4(aq)}$, $NH_4NO_{3(aq)}$, or $NaCl_{(aq)}$, respectively.

Fig. 4*B* shows σ(*RH*) plotted as a function of δ_{AS}, δ_{AN}, and δ_{SC} (see Table S2 for numerical values). For comparison, the isochemical points ($\delta = 0$) are also included in Fig. 4*B* and all lie in an overlapping region near the origin. The point for $NaBr_{(CN)}$–$NaCl_{(aq)}$ (CERH = 50%, σ(*RH*)=0.81, $\delta_{SC} = 0.03$) is not shown because $NaBr_{(CN)}$ particles are expected to be deliquesced above ~45–48% RH (2, 12), thus negating the influence of the NaBr crystal lattice structure. In this instance, $NaCl_{(aq)}$ efflorescence may have been induced by undissolved $NaBr_{(CN)}$ particulate (12), ionic interactions (25), or the collision itself (17). (See *SI Additional Discussion* for more details). However, for the majority of CN–droplet pairs, δ is a good first-order approximation of σ(*RH*) (and thus CERH). Small lattice mismatches ($\delta < 0.12$) generally indicate an effective heterogeneous nucleus [i.e., low σ(*RH*) and high CERH]. Notably, the high $K_2SO_{4(CN)}$–$(NH_4)_2SO_{4(aq)}$ CERH of 77% ($\delta_{AS} = 0.03$) clearly demonstrates that a low δ can lead to a profound effect and offers experimental support for simulations that suggest a small lattice mismatch may be more favorable than a perfect lattice match for nucleation on a heterochemical surface because the crystal nucleus does not necessarily have the same lattice constants as the bulk crystal (23). Larger lattice mismatches ($\delta \gtrsim 0.12$) generally indicate a less effective heterogeneous nucleus. These observations are consistent with previous studies that suggest nucleation is no longer epitaxial (i.e., oriented by crystal lattice structure) at an absolute mismatch greater than ~10–15% (23, 24). However, there were exceptions to these generalizations for $NH_4NO_{3(aq)}$ contact efflorescence, where $NaCl_{(CN)}$ had the lowest lattice mismatch ($\delta_{AN} = 0.03$) but was not the most effective CN. $K_2SO_{4(CN)}$ and $(NH_4)_2SO_{4(CN)}$ were both slightly more effective than $NaCl_{(CN)}$ despite larger lattice mismatches (δ_{AN} =0.18 and 0.22, respectively). In these instances, NH_4NO_3 nucleation may have been influenced by ionic interactions or a crystal face not considered here when calculating δ.

Although a small lattice mismatch appears to have the largest overall effect on CERH for the CN–droplet pairs used in the present study, other factors, such as the DRH of the CN, also influenced the CERH, as exemplified with $NaBr_{(CN)}$–$NaCl_{(aq)}$ contact efflorescence. However, as shown in Fig. S4, there is no overall correlation between σ(*RH*) and the DRH, solubility, or heat of dissolution of the CN. Although there is no clear trend when considering the properties of the CN alone, ionic interactions between the droplet and CN solute may be an important factor on a case-by-case basis. The properties of a solute mixture differ from those of the individual components as a result of, e.g., the common-ion effect and short-range ionic interactions (2, 13, 25–27). For example, nucleation of NaCl can be induced during dissolution of $KCl_{(s)}$ in bulk solutions (26). Thus, the $KCl_{(CN)}$–$NaCl_{(aq)}$ CERH may have been influenced by $KCl_{(CN)}$ dissolution as well as the small lattice mismatch ($\delta_{SC} = 0.11$). Indeed, CN dissolution is possible to some extent before the onset of

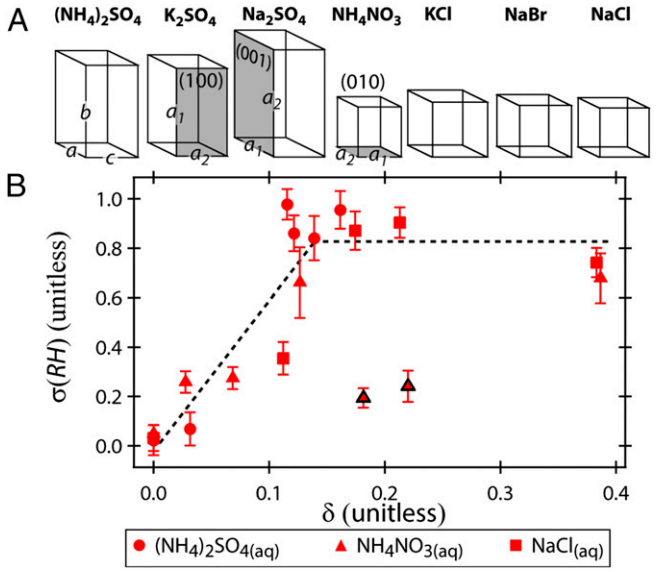

Fig. 4. (*A*) Scaled representations of the unit cell structures for the crystalline compounds used in the present study. The orientation of the unit cell constants *a*, *b*, and *c* are depicted on $(NH_4)_2SO_4$. The orientation of the (100), (001), and (010) crystal faces are demonstrated on K_2SO_4, Na_2SO_4, and NH_4NO_3, respectively. The values for the lattice constants a_1 and a_2 correspond to the values of *a*, *b*, or *c* (e.g., for (100), $a_1 = b$ and $a_2 = c$). (*B*) The σ(*RH*) plotted as a function of δ for all three aqueous compositions. In general, effective CN (i.e., σ(*RH*) < 0.4) had values of $\delta < 0.12$, and less effective CN had values of >0.12. This trend is indicated by the dashed line. The two CN–droplet pairs that do not follow this trend are outlined in black.

Table 1. Parameters used to estimate the *e*-folding times (τ_{col}) for aqueous particles to undergo a collision with potential CN

Scenario	CN source	N_{CN}, cm^{-3}	$D_{p,CN}$, μm	$D_{p,aq}$, μm	K, $cm^3 \cdot s^{-1}$	τ_{col}, s
$D_{p,aq} >> D_{p,CN}$	$(NH_4)_2SO_4$ particle formation event (30)	1.5×10^5	0.01	1	3.4×10^{-7}	20
	urban (36)*	5×10^4	0.04	1	2.4×10^{-8}	850 [14 min]
	remote continental (36)	5×10^3	0.1	1	5.0×10^{-9}	4×10^4 [11 h]
	wildfire BBA (34)*	4×10^4	0.15	1	3.5×10^{-9}	7×10^3 [2 h]
	marine ultrafine SSA (31)*	100	0.05	1	2.0×10^{-8}	5×10^5 [6 d]
$D_{p,aq} << D_{p,CN}$	urban (36)	900	0.6	0.04	1.5×10^{-8}	7.5×10^4 [21 h]
	remote continental (36)/marine SSA (31)	10	1	0.04	2.4×10^{-8}	4×10^6 [48 d]
$D_{p,liq} \approx D_{p,sol}$	urban (36)†	2.5×10^4	0.04	0.05	3.8×10^{-9}	1×10^4 [3 h]
	remote continental (36)†	2.5×10^3	0.1	0.1	1.5×10^{-9}	2.3×10^5 [3 d]
	wildfire BBA (34)	4×10^4	0.15	0.1	1.8×10^{-9}	1.4×10^4 [4 h]

*Urban, wildfire BBA, and ultrafine SSA are illustrated in Fig. 5 processes A, B, and C, respectively, for particle collision scenarios where $D_{p,aq} >> D_{p,CN}$.
†Assuming half of particles are solid (i.e., potential CN).

efflorescence because the droplets are unsaturated with respect to the CN solute. Another important consideration is the mechanical effect of the collision. Niehaus and Cantrell (17) have demonstrated that a solid surface is not necessary to induce ice nucleation upon contact, consistent with our observations of $NaBr_{(CN)}$–$NaCl_{(aq)}$ contact efflorescence. A similar effect may be occurring here, particularly if salt crystal nucleation preferentially occurs at the surface of the droplet, as has been suggested (28). This points toward the possibility of efflorescence induced by amorphous (noncrystalline) aerosol.

Atmospheric Implications. Atmospheric aerosol can contain significant fractions of the inorganic components used in the present study. In urban and remote regions, the dominant inorganic components are NH_4^+, SO_4^{2-}, and NO_3^-, which are largely present as a result of secondary conversion of gaseous NH_3, SO_2, and NO_X emissions, respectively, and can exist as aqueous droplets or as solid particles, depending on ambient conditions and mechanism of formation (2, 11, 20, 29, 30). $(NH_4)SO_4$ has also been implicated in new particle formation events in some urban locations (30). In marine and coastal regions, Na^+ and Cl^- can be found in high amounts due to sea spray aerosol (SSA), which can homogeneously effloresce at ∼44% RH (4, 20, 31, 32). SSA also contains SO_4^{2-}, Br^-, K^+, NH_4^+, and NO_3^-. Additionally, biomass burning aerosol (BBA) can contain discrete $KCl_{(s)}$ and $K_2SO_{4(s)}$ crystal inclusions (33), compounds shown in the present study to be effective CN for efflorescence of $NaCl_{(aq)}$, $NH_4NO_{3(aq)}$, and $(NH_4)_2SO_{4(aq)}$. (See *SI Additional Discussion* for further details of how the model aerosol used in the present study compares to ambient aerosol.) Many coastal regions such as the Los Angeles basin and surrounding areas of Southern California (United States) experience high levels of particulate matter with contributions from SSA (32), anthropogenic emissions (29), recurrent large-scale wildfires (34), and mineral dust (35). Such regions can also experience extreme variations in ambient RH during, e.g., Santa Ana wind events (meteorological events characterized by strong, arid winds originating from inland locations) (34, 35). The mixing of aerosol under changing RH conditions leaves open the possibility for contact efflorescence.

Ultimately, any potential relevance of contact efflorescence is dependent on the probability of a collision between particles at a suitable RH. Thus, contact efflorescence is most likely to be important where the particle number concentrations are high. In urban polluted areas, number concentrations typically exceed 10^4 cm^{-3} and can reach even higher levels during, e.g., new particle formation (30) and biomass burning events (34), with the highest-number concentrations typically being for ultrafine particles (particles with diameters less than ∼100 nm) (3, 20, 29, 36). For a monodisperse population of aqueous particles with diameter $D_{p,aq}$ externally mixed with a monodisperse population of solid CN with diameter $D_{p,CN}$, the *e*-folding time (τ_{col}) for the aqueous particles to undergo a solid–liquid collision is estimated as $\tau_{col} = (KN_{CN})^{-1}$, where N_{CN} is the number concentration of the CN and K is the coagulation coefficient (see *SI Materials and Methods* and Table S3) (20). The τ_{col} can be compared with the typical atmospheric lifetime of an aqueous particle to evaluate whether particle collisions can occur on a relevant timescale. [Note that τ_{col} for ambient aerosol will depend on the true size distribution. Furthermore, additional

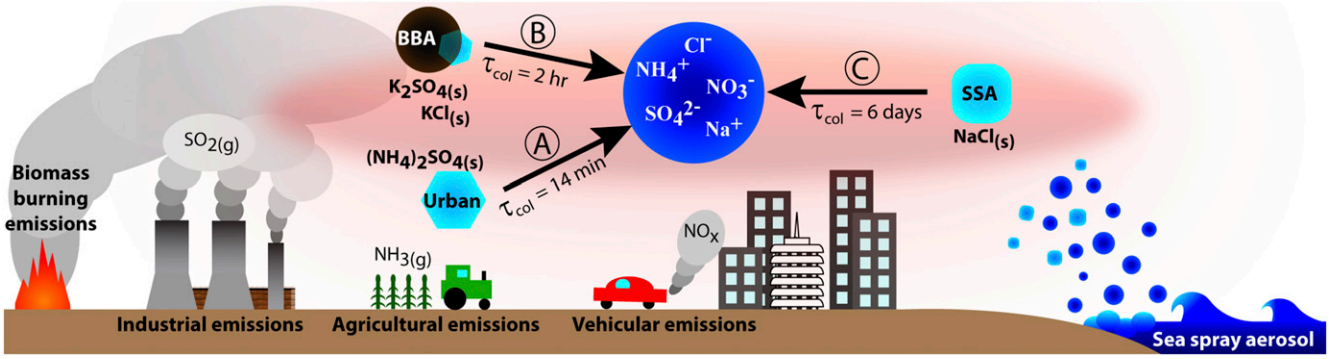

Fig. 5. A depiction of an urban coastal region to illustrate particle collision scenarios where $D_{p,aq} >> D_{p,CN}$. The aqueous phase ($D_{p,aq}$ = 1 μm) is represented by processed SSA (primarily $NaCl_{(aq)}$ when emitted) with accumulated SO_4^{2-}, NO_3^-, and NH_4^+ via secondary aqueous-phase conversion of $SO_{2(g)}$ (industrial emissions), NO_x (vehicular emissions) and $NH_{3(g)}$ (agricultural emissions), respectively, during transport inland. In process A, urban ultrafine particles ($D_{p,CN}$ = 0.04 μm) can contain $(NH_4)_2SO_{4(s)}$ and coexist with the aqueous droplet as a result of secondary processes; τ_{col} is short compared with the lifetime of the aqueous particle. (Refer to Table 1 for parameters used to calculate τ_{col}.) In process B, wildfire BBA ($D_{p,CN}$ = 0.15 μm) can contain discrete $KCl_{(s)}$ and $K_2SO_{4(s)}$ crystal inclusions; during wildfire events, τ_{col} can be well within the lifetime of the aqueous particle. In process C, effloresced ultrafine SSA ($D_{p,CN}$ = 0.05 μm) can contain $NaCl_{(s)}$ and coexist with the aqueous droplet as a result of the hydration hysteresis effect; τ_{col} can be comparable to the lifetime of the aqueous particle.

factors such as electroscavenging, diffusiophoresis, and thermophoresis can increase or decrease the number of particle collisions (37).] K varies strongly as a function of $D_{p,aq}$ and $D_{p,CN}$ (20). Thus, due to the wide range of particle sizes in the atmosphere, τ_{col} can vary greatly depending on location and particle sources, as shown in Table 1 and discussed for scenarios where $D_{p,aq} >> D_{p,CN}$, $D_{p,aq} << D_{p,CN}$, and $D_{p,aq} \approx D_{p,CN}$.

$D_{p,aq} >> D_{p,CN}$. Fig. 5 illustrates τ_{col} for large aqueous inorganic aerosol (~1 μm diameter) from, e.g., SSA and fog droplet processing to undergo a collision with a potential CN (4, 20, 32, 36). If contact efflorescence occurs, the resulting water loss and change in morphology would influence the chemical reactivity, atmospheric lifetime, and optical properties of the large particle. If all potential CN are assumed to be solid or contain solid material, τ_{col} ranges from seconds at high number concentrations ($N_{CN} = 10^5$ cm^{-3}) to days at lower number concentrations ($N_{CN} = 10^2$ cm^{-3}). The typical atmospheric lifetime for a 1-μm particle ranges from days to weeks (20). Thus, τ_{col} can be well within an atmospherically relevant timescale even if only a fraction of potential CN contain solid material.

$D_{p,aq} << D_{p,CN}$. A substantial number of liquid–solid collisions can also occur between a large solid particle and ultrafine aqueous particles (18, 19). Contact efflorescence could potentially occur in this scenario, as well. For example, urban ultrafine $NH_4NO_{3\,(aq)}$ particles could effloresce upon contact with a solid SSA particle. In this scenario, τ_{col} is on the order of days to months, suggesting a substantial impact on total aerosol liquid water content only during high-number concentrations of large solid particles. However, even at low-number concentrations, contact efflorescence may still be important to consider for its influence on the surface properties of the large CN. As multiple collisions occur, the solid particle may develop a crystalline coating, which could influence the aging process and thus the particle shape, composition, and optical properties of the CN.

$D_{p,aq} \approx D_{p,CN}$. Diurnal variations in ambient RH and the hydration hysteresis effect can lead to the coexistence of solid and liquid particles with the same source and similar size distributions (11, 19). Coagulation coefficients become lowest when particle diameters are similar, but τ_{col} can still be within relevant timescales for ultrafine particles when number concentrations are $\geq 10^3$ cm^{-3}.

Concluding Remarks

This study has established that contact efflorescence is a pathway for crystallization of microdroplets at high RH and that particle collisions can occur on atmospherically relevant timescales. Although contact efflorescence may be situational in some scenarios (e.g., during wildfire events and arid meteorological conditions), the effects would persist for a longer period because the effloresced particle will remain crystalline for as long as the ambient RH is below the DRH of the inorganic component. Considering these observations and the prevalence of soluble inorganic material in atmospheric particulate, contact efflorescence may be a potentially important process occurring in the atmosphere.

ACKNOWLEDGMENTS. This work was supported by the National Science Foundation (Grant AGS1506691). R.D.D. acknowledges a NASA Earth and Space Science Fellowship (NNX13AN69H).

1. Sear RP (2012) The non-classical nucleation of crystals: microscopic mechanisms and applications to molecular crystals, ice and calcium carbonate. *Int Mater Rev* 57(6):328–356.
2. Martin ST (2000) Phase transitions of aqueous atmospheric particles. *Chem Rev* 100(9): 3403–3454.
3. DeMott PJ, et al. (2010) Predicting global atmospheric ice nuclei distributions and their impacts on climate. *Proc Natl Acad Sci USA* 107(25):11217–11222.
4. Finlayson-Pitts BJ (2003) The tropospheric chemistry of sea salt: A molecular-level view of the chemistry of NaCl and NaBr. *Chem Rev* 103(12):4801–4822.
5. Haywood J, Boucher O (2000) Estimates of the direct and indirect radiative forcing due to tropospheric aerosols: A review. *Rev Geophys* 38(4):513–543.
6. IPCC (2013) *Climate Change 2013—The Physical Science Basis: Contribution of Working Group I to the Fifth Assessment Report of the IPCC* (Cambridge Univ Press, Cambridge, UK).
7. Wang J, Jacob DJ, Martin ST (2008) Sensitivity of sulfate direct climate forcing to the hysteresis of particle phase transitions. *J Geophys Res* 113(D11):D11207.
8. Pant A, Parsons MT, Bertram AK (2006) Crystallization of aqueous ammonium sulfate particles internally mixed with soot and kaolinite: Crystallization relative humidities and nucleation rates. *J Phys Chem A* 110(28):8701–8709.
9. Hung H-M, Martin ST (2002) Size effect of hematite and corundum inclusions on the efflorescence relative humidities of aqueous ammonium nitrate particles. *J Geophys Res* 107(D10):4086.
10. Mikhailov E, Vlasenko S, Niessner R, Pöschl U (2004) Interaction of aerosol particles composed of protein and salts with water vapor: Hygroscopic growth and microstructural rearrangement. *Atmos Chem Phys* 4(2):323–350.
11. Zaveri R, Barnard J, Easter R, Riemer N, West M (2010) Particle-resolved simulation of aerosol size, composition, mixing state, and the associated optical and cloud condensation nuclei activation properties in an evolving urban plume. *J Geophys Res* 115(D17):D17210.
12. Davis RD, Lance S, Gordon JA, Tolbert MA (2015) Long working-distance optical trap for in situ analysis of contact-induced phase transformations. *Anal Chem* 87(12):6186–6194.
13. Wexler A, Clegg S (2002) Atmospheric aerosol models for systems including the ions H^+, NH_4^+, Na^+, SO_4^{2-}, NO_3^-, Cl^-, Br^-, and H_2O. *J Geophys Res* 107(D14):4207.
14. Shindell D, et al. (2013) Radiative forcing in the ACCMIP historical and future climate simulations. *Atmos Chem Phys* 13(6):2939–2974.
15. Yu P, et al. (2015) Evaluations of tropospheric aerosol properties simulated by the Community Earth System Model with a sectional aerosol microphysics scheme. *J Adv Model Earth Syst* 7(2):865–914.
16. Moreno L, Stetzer O, Lohmann U (2013) Contact freezing: A review of experimental studies. *Atmos Chem Phys* 13(19):9745–9769.
17. Niehaus J, Cantrell W (2015) Contact freezing of water by salts. *J Phys Chem Lett* 6(17):3490–3495.
18. Tsai I, Chen J, Lin Y, Chou C, Chen W (2015) Numerical investigation of the coagulation mixing between dust and hygroscopic aerosol particles and its impacts. *J Geophys Res* 120(9):4213–4233.
19. Jacobson M (2002) Analysis of aerosol interactions with numerical techniques for solving coagulation, nucleation, condensation, dissolution, and reversible chemistry among multiple size distributions. *J Geophys Res* 107(D19):4366.
20. Seinfeld JH, Pandis SN (2006) *Atmospheric Chemistry and Physics* (Wiley-Interscience, Hoboken, NJ), 2nd Ed, pp 284–622.
21. Mullin JW (2001) Crystal growth. *Crystallization* (Butterworth-Heinemann, Oxford), 4th Ed, pp 216–284.
22. Bryant GW, Hallett J, Mason BJ (1960) The epitaxial growth of ice on single-crystalline substrates. *J Phys Chem Solids* 12(2):189–195.
23. Mithen JP, Sear RP (2014) Computer simulation of epitaxial nucleation of a crystal on a crystalline surface. *J Chem Phys* 140(8):084504.
24. van Meel JA, Sear RP, Frenkel D (2010) Design principles for broad-spectrum protein-crystal nucleants with nanoscale pits. *Phys Rev Lett* 105(20):205501.
25. Valdeavella C, Perkyns J, Pettitt B (1994) Investigations into the common ion effect. *J Chem Phys* 101(6):5093–5109.
26. Simon B (1981) Dissolution rates of NaCl and KCl in aqueous solution. *J Cryst Growth* 52(Part 2):789–794.
27. Cohen MD, Flagan RC, Seinfeld JH (1987) Studies of concentrated electrolyte solutions using the electrodynamic balance. 1. Water activities for single-electrolyte solutions. *J Phys Chem* 91(17):4563–4574.
28. Ciobanu VG, Marcolli C, Krieger UK, Zuend A, Peter T (2010) Efflorescence of ammonium sulfate and coated ammonium sulfate particles: Evidence for surface nucleation. *J Phys Chem A* 114(35):9486–9495.
29. Zhang R, et al. (2015) Formation of urban fine particulate matter. *Chem Rev* 115(10): 3803–3855.
30. Crilley LR, et al. (2014) Observations on the formation, growth and chemical composition of aerosols in an urban environment. *Environ Sci Technol* 48(12):6588–6596.
31. Fan T, Toon O (2011) Modeling sea-salt aerosol in a coupled climate and sectional microphysical model: Mass, optical depth and number concentration. *Atmos Chem Phys* 11(9):4587–4610.
32. Adachi K, Buseck P (2015) Changes in shape and composition of sea-salt particles upon aging in an urban atmosphere. *Atmos Environ* 100:1–9.
33. Li J, Pósfai M, Hobbs P, Buseck P (2003) Individual aerosol particles from biomass burning in southern Africa: 2. Compositions and aging of inorganic particles. *J Geophys Res Atmos* 108(D13):8484.
34. Zauscher MD, Wang Y, Moore MJ, Gaston CJ, Prather KA (2013) Air quality impact and physicochemical aging of biomass burning aerosols during the 2007 San Diego wildfires. *Environ Sci Technol* 47(14):7633–7643.
35. Guazzotti S, Whiteaker J, Suess D, Coffee K, Prather K (2001) Real-time measurements of the chemical composition of size-resolved particles during a Santa Ana wind episode, California USA. *Atmos Environ* 35(19):3229–3240.
36. Majeed MA, Wexler AS (2001) Microphysics of aqueous droplets in clouds and fogs as applied to PM-fine modeling. *Atmos Environ* 35(9):1639–1653.
37. Ardon-Dryer K, Huang Y-W, Cziczo DJ (2015) Laboratory studies of the collection efficiency of sub-micrometer aerosol particles by cloud droplets on a single-droplet basis. *Atmos Chem Phys* 15(16):9159–9171.
38. Hillier AC, Ward MD (1996) Epitaxial interactions between molecular overlayers and ordered substrates. *Phys Rev B Condens Matter* 54(19):14037–14051.
39. Gao Y, Chen SB, Yu LE (2006) Efflorescence relative humidity for ammonium sulfate particles. *J Phys Chem A* 110(24):7602–7608.
40. Bodsworth A, Zobrist B, Bertram AK (2010) Inhibition of efflorescence in mixed organic–inorganic particles at temperatures less than 250 K. *Phys Chem Chem Phys* 12(38):12259–12266.